Research

Metal–organic framework mediated Ni-deposition on MWCNTs for direct methanol fuel cell catalysis

Reham Shams-Eldin[1] · Aya A. Ali[1] · Amal Hani[1] · Rana R. Haikal[1] · Hussein M. Fahmy[2] · Rasha M. El Nashar[2] · Mohamed H. Alkordi[1]

Received: 24 March 2023 / Accepted: 15 May 2023
Published online: 25 May 2023

Abstract
Herein, we present the utilization of Ni^{2+}-doped, amine-functionalized, UiO-66-NH_2 metal–organic framework (MOF) nanoparticles deposited onto multi-walled carbon nanotubes (MWCNTs) as a precursor to generate electrocatalytically active catalyst towards methanol (MeOH) oxidation. The electrode material displayed an onset potential of 0.42 V (vs Hg/HgO) with maximum activity at 1 M MeOH concentration (143 mA/cm^2 current density at 0.6 V vs Hg/HgO). The catalyst also demonstrated high stability, retaining 93.5% of its initial activity under continuous electrolysis for 1 h, and 84.1% after 10 h.

Keywords Metal-organic frameworks · Carbon nanotubes · Electrocatalysis · Methanol oxidation · Composite

1 Introduction

Elevated greenhouse gas emissions, resulting from heavy dependence on fossil fuels, have adversely impacted the global climate. Therefore, a great interest has developed among scientists to implement greener technologies to shift the global energy situation towards a more sustainable model, utilizing energy sources with less carbon footprint [1].

Methanol is a feedstock chemical with relatively high energy density that can be used as a fuel in direct methanol fuel cells (DMFCs), with far enhanced efficiency as compared to internal combustion engines [2]. The vast majority of such DMFCs utilize Pt as the catalyst on both the anode (methanol oxidation reaction) and the cathode (oxygen reduction reaction) electrodes. Due to the high cost and limited abundance of Pt, catalysts based on non-precious group elements (NPG) are of high interest [3]. The use of NPG catalysts in DMFCs is hindered by the catalyst poisoning and the slow methanol electro-oxidation kinetics at the anodes utilizing NPGs catalysts [2]. Therefore, developing an NPG-based electrocatalyst for methanol oxidation in DMFCs that demonstrates (i) low overpotential, (ii) rapid kinetics, and (iii) maintained activity for prolonged reaction time is of prime interest [3]

The methanol electro-oxidation reaction is categorized based on the supporting electrolyte pH (acidic and alkaline). Alkaline medium prevails over acidic medium in offering faster oxidation kinetics [4, 5] due to facilitated alkoxide ion production at high pH, as pointed out by Kwon and co-workers in their study of the direct effect of base concentration on methanol electro-oxidation kinetics [6]. Despite the fact that methanol electro-oxidation has a thermodynamic potential of 0.03 V (vs. SHE), this value is not realizable even with the best catalysts due to the number of electrons involved in this step [7]. Precious metals such as Pt [8–10], Au [11–13], and Ag [14] demonstrate high catalytic activity for electro-oxidation of

✉ Mohamed H. Alkordi, malkordi@zewailcity.edu.eg | [1]Center for Materials Science, Zewail City of Science and Technology, Giza 12578, Egypt. [2]Chemistry Department, Faculty of Science, Cairo University, Giza 12613, Egypt.

short-chained alcohols at potentials below 1.0 V, however, their elevated cost and their relatively low abundance preclude their use in commercial DMFCs. Alternative anodic modifiers utilizing NPG metals, especially those based on Co^{2+}, Ni^{2+}, and Cu^{2+}, are currently of great interest as redox mediators for the methanol electro-oxidation reactions in alkaline media [15]. For such NPG catalysts, it is argued that the catalytic activity is ascribed to the generation of oxidative M^{3+} species ($M^{3+} = Co^{3+}$, Ni^{3+}, or Cu^{3+}) along the reaction pathway, as key intermediates to facilitate their catalytic activity towards methanol oxidation. For example, A. Gopalakrishnan and his colleagues have prepared MoS_2 nanostructure supported on Ni foam (MoS_2/NF-5) via a hydrothermal method, which demonstrated activity towards methanol oxidation up to 73 mA/cm^2 at 0.7 V vs RHE in 0.1 M KOH and 0.5 M methanol at a scan rate of 30 mV/s [16].

Electrochemically active catalysts based on metal–organic frameworks (MOFs) have specifically gained significant interest in recent years as potential NPG porous catalysts with superior performance. MOFs are considered novel microporous hybrid inorganic–organic solids with promising activities in numerous demanding applications [17]. The utilization of MOFs in DMFCs as heterogeneous catalysts is attributed to their defined pore size [18] and ability to adsorb methanol species on their surface. Their high specific surface areas can as well accommodate the generated intermediate species through physical adsorption, at which the intermediates will subsequently react in two-step reactions to reach CO_2 as the final product [7]. Several hypotheses have been presented in literature to explain the methanol oxidation catalytic activity at the MOF surfaces. Fleischmann and co-workers suggested MeOH oxidation proceeds through formation of $M^{3+}OOH$ species (M = Co, Ni, or Cu) from metal hydroxides [19]. The $M^{3+}OOH$ species serve as redox mediators for methanol electro-oxidation in alkaline media. Fleischmann proposed the adsorption of methanol substrate on M^{3+} species to provoke radical intermediates, which will further interact with M^{3+} species and produce M^{2+} species along with other oxidation products. In a separate study by Wang and co-workers, Ni complexes demonstrated involvement of the Ni^{2+}/Ni^{3+} redox pair throughout the methanol oxidation process[20]. Nonetheless, pristine MOFs as anodic modifiers in DMFCs are rarely reported accounting for their modest electrical conductivity regulated by the poor overlap between valence orbitals and the electronic states on metal ions and ligands [21–23]. As a result, pristine MOFs demonstrated reduced current densities when utilized in DMFCs.

Despite the high surface area of MOFs, it suffers from low electrical conductivity, which is essential for electrocatalytic applications, therefore one strategy is to utilize a conductive support in order to enhance the catalyst conductivity [24–26]. Alternatively, MOFs were rather utilized as precursors or hard templates for the synthesis of homogenously dispersed metal/metal oxides on porous carbon under pyrolysis at different temperatures to enhance their electrical conductivity. For example, Rezaee and co-workers reported NiCo/NiO-CoO/nanoporous carbon as a redox mediator for methanol oxidation through direct pyrolysis of bimetallic NiCo-MOF [27]. Such composite exhibited a maximum current density of 185 mA/cm^2 at 0.65 V vs. Ag/AgCl. Similarly, Qian et al. pyrolyzed Ni^{2+}/Co^{2+} MOF using an organic linker L-aspartic acid in air at 300 °C to achieve NF/Co_3O_4/$NiCo_2O_4$ with nano-spindle arrays morphology [28]. The calcination process of Ni^{2+}/Co^{2+} ensured fast diffusion rates of electrolyte ions to the accessible active sites, thereby enhancing its electrocatalytic activity towards methanol oxidation. Moreover, Sheikhi and co-workers fabricated a zirconium oxide-based porous carbonaceous platform as a support for Ni nanoparticles through MOF calcination at 800 °C [29]. Despite the exceptional electrocatalytic performance, nevertheless, such synthetic strategy is energy-consuming, which could limit its large-scale application. In this regard, for successful commercially applicable DMFCs, further exploitation is required to approach an economic synthesis procedures of MOFs catalysts at a large scale.

To approach the inherent issue of MOFs' low electrical conductivity, conductive carbon supports such as, graphene or its derivatives, carbon nanotubes and activated carbon are incorporated to construct MOF composites with adequate electrical conductivity for electrocatalytic applications [30]. For example, a composite of Co-benzenedicarboxylate MOF with 5 wt% graphene oxide (Co-BDC MOF@5wt% GO) exhibited a current density of 291 mA/cm^2 at 1.77 V vs. RHE in 1 M KOH and 3 M MeOH [31]. Similarly, a current density of 130 mA/cm^2 at 1.59 V vs. RHE was attained using Co-benzenetricarboxylate MOF with 1 wt% reduced graphene oxide (Co-BTC MOF@1wt% rGO) in 1 M NaOH and 2 M MeOH [32]. Despite the enhanced conductivity of rGO, increasing its amount in the composite in fact reduced the attained current density due to sheets restacking and blocking of MOF active sites, and hindering methanol oxidation at surface that is now occupied by the hydroxyl groups that is found in the alkaline media [30]. Another examples of Ni-benzenetricarboxylate MOF and reduced graphene oxide composite (Ni-BTC MOF@4wt% rGO) demonstrated a current density of 200.22 mA/cm^2 at 1.61 V vs. RHE in 1 M NaOH and 2 M MeOH [26]. The observed improvement in electrocatalytic performance of MOF-graphene oxide composites towards methanol oxidation is attributed to the synergy between conductivity of graphene oxide sheets and the high surface area and catalytic activity of MOF.

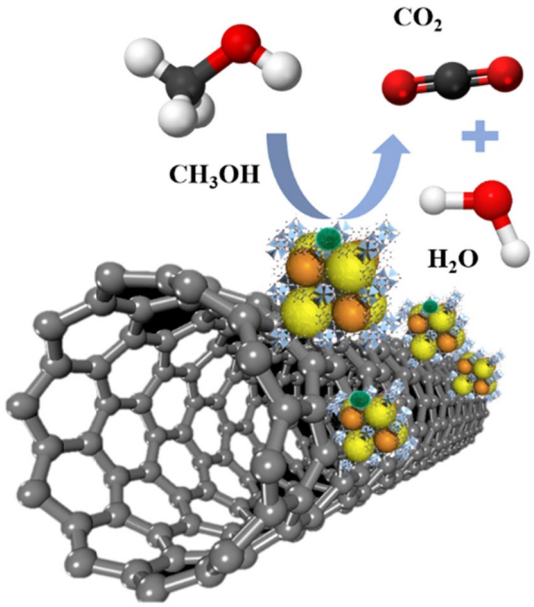

Scheme 1 In-situ deposition of MOF@MWCNTs as a precursor to $Ni(OH)_2$ active catalyst for methanol oxidation

Herein, we utilized Ni-UiO-66-NH_2@MWCNTs through simple incipient wetness impregnation method. The MOF@MWCNTs provides a platform for efficient deposition of $Ni(OH)_2$@MWCNTs, with notable activity towards methanol oxidation in an alkaline medium at low onset potential through MOF degradation and dispersion of nickel hydroxide nanoparticles on 1D MWCNTs support, Scheme 1.

2 Experimental and methods

All reagents of commercial grade were used without any further purification. Electrochemical measurments were done in three electrode system using reference electrode (RE-61AP) Hg/HgO filled with 1 M NaOH (from ALS Instruments) and data was recorde using EC-Lab software, graphite rod as counter electrode and glassy carbon electrode as working electrode. FTIR was measured using ThermoScientificiS10 spectrophotometer. $ZrCl_4$ anhydrous > 98%, 2-aminoterephthalic acid 99%, HCl 37% were purchased from Acros Organics. N,N'dimethylformamide (DMF) analytical reagent grade 99.99%, Methanol 99% HPLC grade and acetonitrile (ACN) HPLC grade were purchased from Fisher Scientific-UK Chemicals. $Ni(NO_3)_2.6H_2O$ 98% was purchased from Alfa Aesar from USA, KOH 90% from PioChem Egypt, Carboxylated multi-walled carbon nanotubes (MWCNT-COOH) > 95 wt%/30–50 nm was purchased from Cheap Tubes (SKU:050306) were used as received without further purification.

2.1 Synthesis of Ni-UiO-66-NH2@MWCNTs

In this work, Ni-UiO-66-NH_2@MWCNTs, as an electrochemical catalyst for methanol oxidation, was prepared according to our previously reported work [33]. Briefly,in two clean separate vials, 42.5 mg (0.18 mmol) of $ZrCl_4$ was suspensed in 5 mL DMF and 1 mL HCl (37%) (Solution A), while 45.5 mg (0.428 mmol) of 2-aminoterphethalic acid and 50 mg of MWCNTs-COOH were suspensed in 10 ml DMF (Solution B). Both solutions were left to sonicate for 20 min. Solution A was added to solution B while stirring at 400 rpm with a magnetic bar. The vial was capped and left under stirring at 80 °C overnight. The as-prepared MOF@MWCNTs was filterd, washed and left to exchange in ACN at 85 °C for 2 h, then the solid was filtered and dried overnight at 80 °C. For Ni-metallation, 50 mg of the UiO-66-NH_2@MWCNTs was suspensed in 5 ml acetonitrile, followed by addition of 15.2 mg $Ni(NO_3)_2.6H_2O$ to the solution and sonication for 20 min. The vial was transferred to thermalblock and dried while stirring at 85 °C. The temperature was then raised to 120 °C to ensure complete evaporation of acetontitrile. The synthetic process is represented and summarized in Scheme 2.

2.2 Electrochemical measurements

About 8 mg of Ni-UiO-66-NH_2@MWCNTs was dispersed in 1 ml of isopropanol followed by the addition of 7 µl of Nafion (10 wt% in isopropanol). The ink was sonicated then 20 µl were drop-casted on a glassy carbon electrode and left to dry at room temperature. The cyclic voltametry (CV), impedance (EIS) and chronoamperometry measurements were performed in 1 M KOH solution as supporting electrolyte at room temperature from 0 to 0.6 V vs Hg/HgO at scan rates ranging from 5 to 100 mV/s. EIS measurements were performed by using a voltage amplitude of 10 mV and frequencies from 0.1 Hz to 10^5 Hz.

3 Results and discussion

To confirm the successful deposition of UiO-66-NH_2 MOF nanoparticles (NPs) atop the MWCNTs, Fourier-transform infrared (FTIR) spectroscopy was utilized (Fig. 1a), where the MOF characteristic peaks were evident in the FTIR spectrum of the UiO-66-NH_2@MWCNTs and Ni-UiO-66-NH_2@MWCNTs composite. The peaks at 1575 cm^{-1} and 1432 cm^{-1} correspond to the stretching vibration

Scheme 2 A pictorial representation of the synthetic process

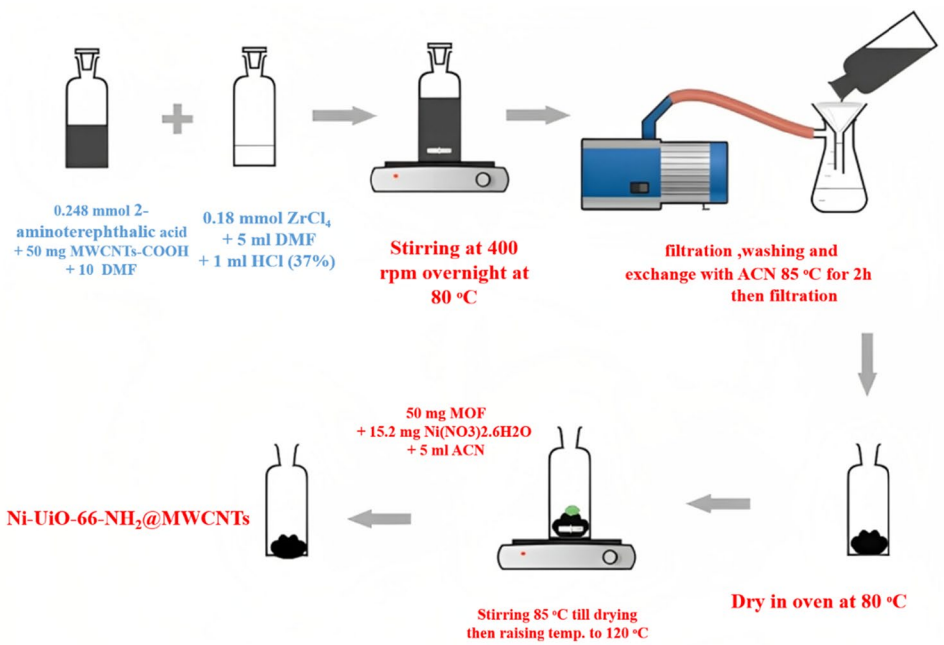

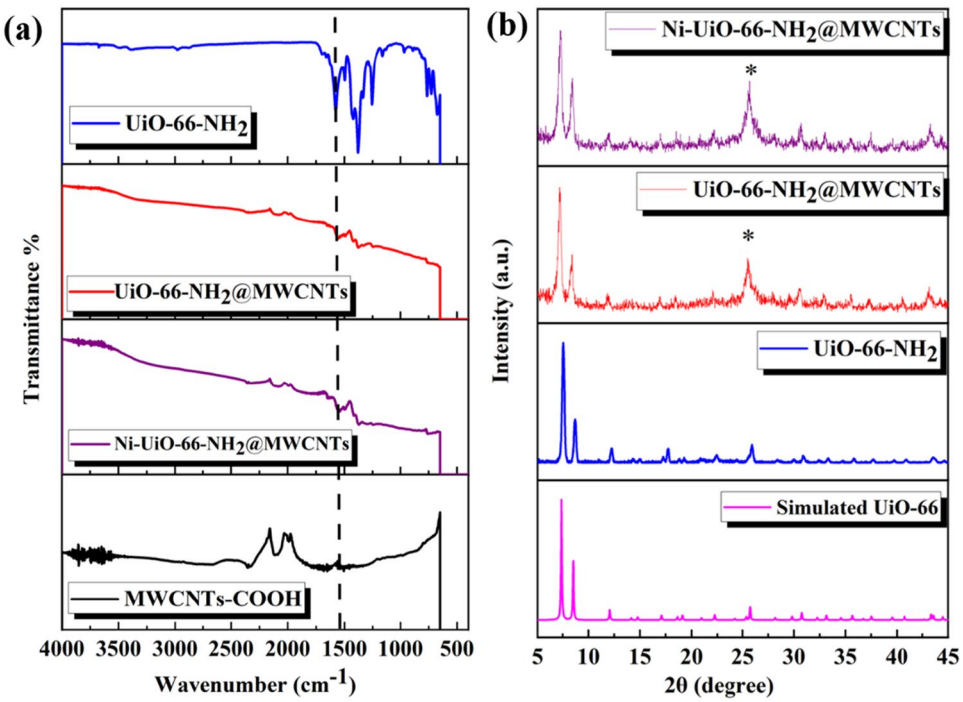

Fig. 1 (**a**) FTIR spectra of UiO-66-NH_2, UiO-66-NH_2@MWCNTs, Ni-UiO-66-NH_2@MWCNTs, and MWCNTs-COOH and (**b**) XRD diffraction patterns of UiO-66-NH_2, UiO-66-NH_2@MWCNTs, Ni-UiO-66-NH_2@MWCNTs, and simulated UiO-66. The asterisk (*) demonstrates the additional peak representing the (002) planes of MWCNTs

frequencies of C=O and C=C of the 2-aminoterephthalic acid ligand, respectively, which are absent in the MWCNTs-COOH spectrum thereby confirming the successful deposition of MOF NPs atop the MWCNTs-COOH [34]. For further investigation, X-ray diffraction (XRD) was also performed to ensure the successful preparation of UiO-66-NH_2@MWCNTs. As shown in Fig. 1b, the XRD pattern of UiO-66-NH_2@MWCNTs and Ni-UiO-66-NH_2@MWCNTs revealed the characteristic peaks of the pristine MOF. An additional peak at $2\theta = 25.7$ was evident (marked by * in Fig. 1b), which is characteristic of (002) planes of graphitic carbon of MWCNTs [35].

Thermogravimetric analysis (TGA), Fig. 2a, was performed to investigate the thermal stability of the

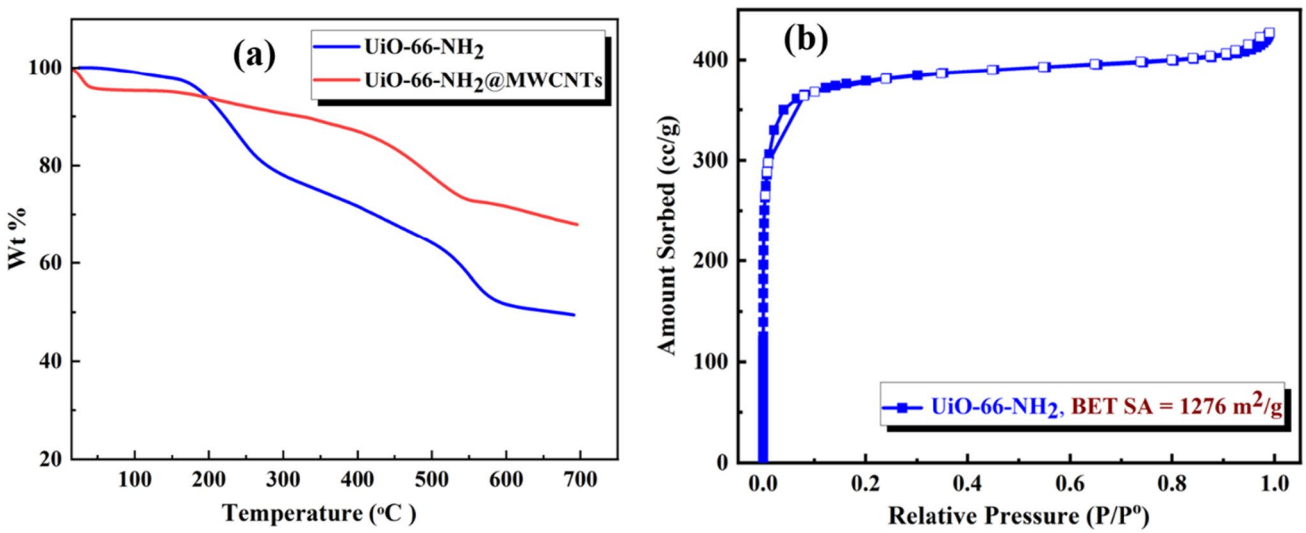

Fig. 2 (**a**) TGA of UiO-66-NH_2 and UiO-66-NH_2@MWCNTs, and (**b**) N_2 sorption isotherms for UiO-66-NH_2

composite. Compared to pristine MOF, the thermal stability of the composite was enhanced, which indicates the strong interaction between MWCNTs-COOH and MOF NPs [36]. To confirm the microporosity of the UiO-66-NH_2 MOF NPs, N_2 sorption isotherm was measured (Fig. 2b), which exhibited Type-I characteristics indicating the presence of micropores. The Brunauer–Emmett–Teller (BET) surface area was calculated to be 1276 m^2/g, which is consistent to previous literature.

Figure 3 shows the scanning electron microscopy (SEM) images of (a) MWCNTs-COOH (b) UiO-66-NH_2@MWCNTs and (c) Ni-UiO-66-NH_2@MWCNTs, which confirm the successful deposition of MOF NPs on the surface of MWCNTs-COOH with uniform coverage.

Energy-dispersive X-ray spectroscopy (EDX) measurements (Fig. 4) were also conducted on the Ni-loaded composite, which revealed the homogeneous distribution of Ni within the composite, as evidenced by the Ni map aligning closely with the elemental maps of C, O, and Zr. Moreover, the analysis indicated that the composite contains 2.7 wt% of Ni.

Metalation of UiO-66-NH_2@MWCNTs with Ni(II) ions was conducted through incipient wetness impregnation, where simply soaking the composite in an acetonitrile solution of $Ni(NO_3)_2$ for 4 h was sufficient to induce metalation by Ni(II) ions. Cyclic voltammetry (CV) of Ni-UiO-66-NH_2@MWCNTs in alkaline medium (1 M KOH) demonstrated well-defined anodic and cathodic peaks of Ni^{2+}/Ni^{3+} redox pair at 0.494 V and 0.352 V vs Hg/HgO respectively, Fig. 5, confirming the inclusion of Ni^{2+} ions within the composite. The current density of this redox couple increased with consecutive CV scans, Fig. 3 inset, indicating the continuous adsorption of OH^- ions to activate

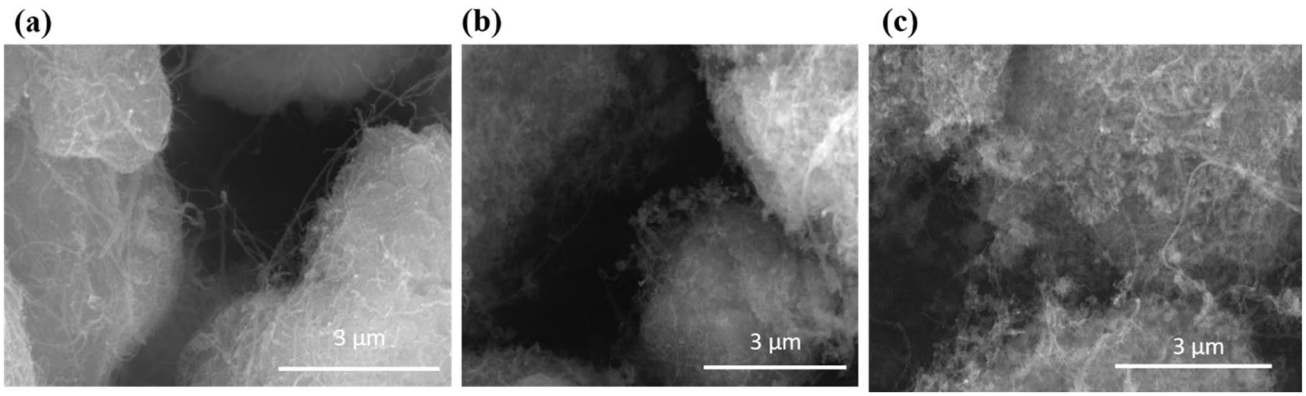

Fig. 3 SEM images at the same magnification of (**a**) MWCNTs-COOH, (**b**) UiO-66-NH_2@MWCNTs and (**c**) Ni-UiO-66-NH_2@MWCNTs

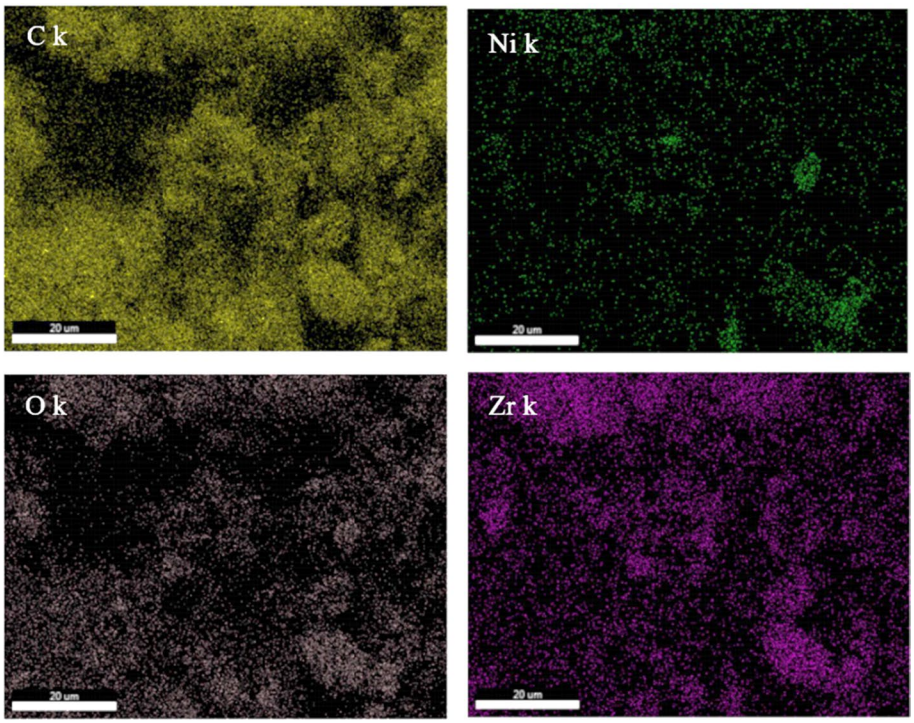

Fig. 4 EDX maps for Ni-UiO-66-NH_2@MWCNTs showing the homogenous distribution of the elements (labeled images) throughout the sample

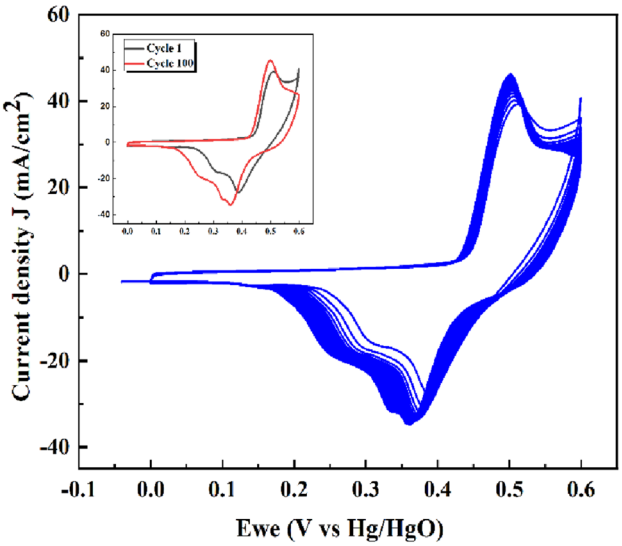

Fig. 5 Activation of Ni-UiO-66-NH_2@MWCNTs in 1 M KOH at scan rate 100 mV/s

Ni-UiO-66-NH_2@MWCNTs and form the electrocatalytically active species NiOOH according to Eq. (1) [29].

$$Ni(OH)_2 + OH^- \rightarrow NiOOH + H_2O + e^- \quad (1)$$

Upon measuring CVs at different scan rates from 5–100 mV/s, the current density increased with increasing the scan rate indicating a diffusion-controlled mechanism. for $Ni(OH)_2$/NiOOH on the electrode surface, Fig. 6a. Figure 6b shows the linear dependency of the anodic current density on square root of the scan rate, which confirms the aforementioned explanation.

In order to assess the electrocatalytic acitivty of Ni-UiO-66-NH_2@MWCNTs towards methanol (MeOH) oxidation, CVs were measured at different alkaline methanolic concentrations, Fig. 7a. The observed current density increases upon increasing the MeOH concentration up to a maximum of 143 mA/cm^2 at 0.6 V (vs Hg/HgO) at 1 M MeOH concentration, beyond which the current density starts to decline (Fig. 7a). This can be ascribed to the increasing availability of.

MeOH to be adsorbed on the abundant active sites. However, beyond 1 M MeOH concentration, there exists no more additional unoccupied active sites as well as the reaction intermediates and unreacted methanol tend to accumulate, thereby decreasing the current density [37]. In order to ensure that the presence of Ni ions is responsible for methanol oxidation catalytic activity, CV was carried out for UiO-66-NH_2@MWCNTs under similar conditions. As shown in Fig. 7b, the current density is negligible and there are no discernible redox peaks contrary to Ni-UiO-66-NH_2@MWCNTs.

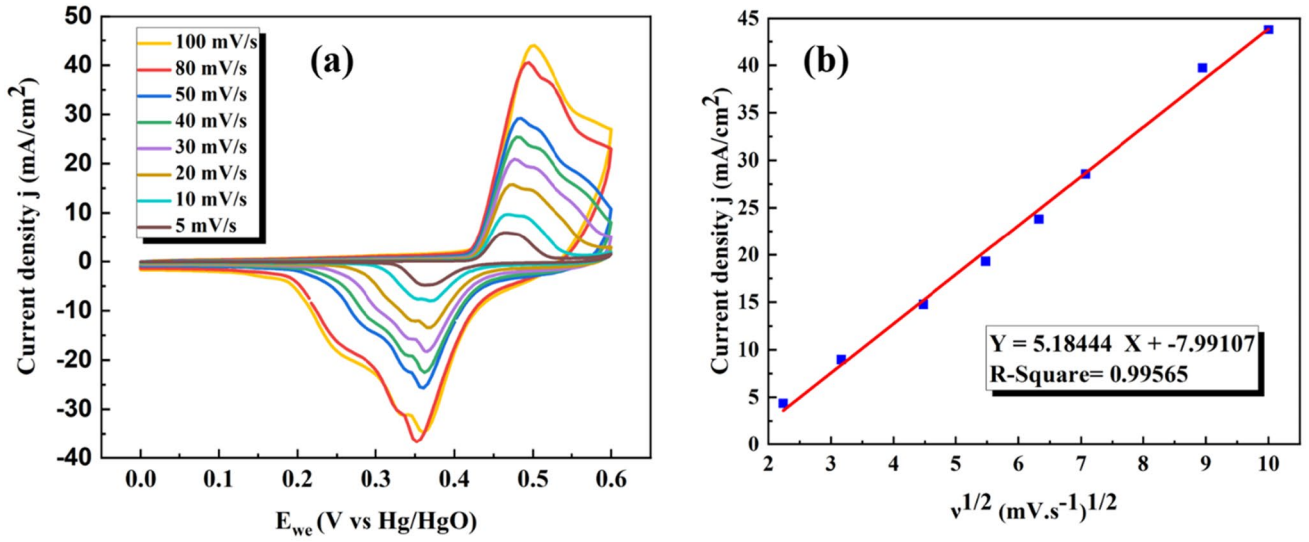

Fig. 6 (**a**) CVs of Ni-UiO-66-NH2@MWCNTs in 1 M KOH at different scan rates and (**b**) linear relationship between anodic current density at 0.49 V and square root of scan rate

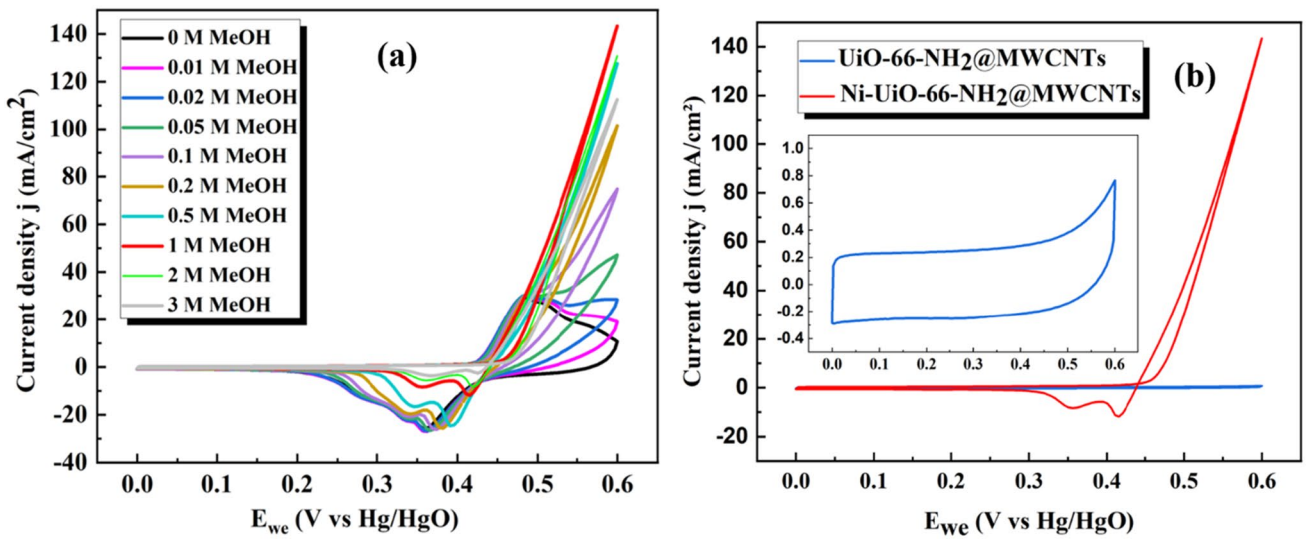

Fig. 7 (**a**) CVs of Ni-UiO-66-NH_2@MWCNTs in 1 M KOH and different methanol concentrations at 50 mV/s scan rate and (**b**) CVs of UiO-66-NH_2@MWCNTs and Ni-UiO-66-NH_2@MWCNTs in 1 M KOH and 1 M MeOH at 50 mV/s scan rate

Overall, the presented catalyst demonstrated superior activity towards methanol oxidation in comparison with other previously reported catalysts as shown in Fig. 8 despite the noted differences in the reported reaction conditions utilized in the previous publications, which are summarized in Table 1. Furthermore, the stability of Ni-UiO-66-NH_2@MWCNTs was investigated by chronoamperometry (CA) in 1 M MeOH/KOH solution at a fixed. potential of 0.6 V vs Hg/HgO for 10 h (Fig. 9a). The high initial current density is most likely due to fast oxidation of adsorbed MeOH on the active sites [38]. The following drop in current density is therefore due to partial depletion of adsorbed MeOH as well as accumulation of adsorbed intermediates like COOH, CHO and CO on the catalyst surface, which may lead to catalyst saturation [39]. Nevertheless, Ni-UiO-66-NH_2@MWCNTs retained 84.1% of the current density after 10 h (Fig. 9b). The slight decrease in current density can be explained by the reduction of

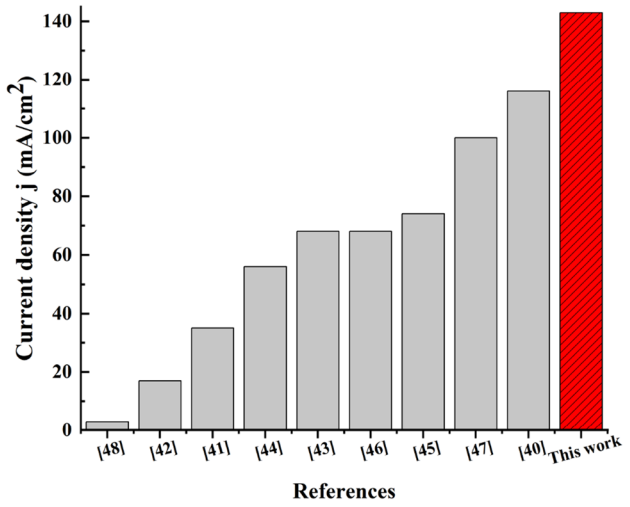

Fig. 8 Current density recorder utilizing the Ni-UiO-66-NH2@MWCNTs, in 1 M Methanol/KOH at 50 mV/s scan rate, as compared to previous literature comparing the values of highest recorded current density

methanol concentration in solution with time after its oxidation on the electrode surface.

In an attempt to gain deeper insight into the proposed mechanism, electrochemical impedence spectroscopy (EIS) was performed for Ni-UiO-66-NH_2@MWCNTs in 1 M KOH before and after addition of 1 M MeOH (Fig. 10). The experimental points were well-fitted to proper equivalent circuits that contain R_{sol}, CPE_{dl}, R_{ct}, CPE_{ads}, R_{ads}, and W as solution resistance, constant phase element for double layer capacitance, charge transfer resistance, constant phase element for adsorption of reaction intermediates on the electrode surface, adsorption of reaction intermediates on the electrode surface resistance, and Warburg impedance, respectively as given in Table 2. As shown in Fig. 10, the Nyquist plots showed significantly different appearances before and after the addition of MeOH to the alkaline electrolyte, which confirmed the methanol oxidation mechanism on the anode follows that proposed by Harrington and Conway [49, 50]. The large semicicle at high frequency in the EIS for the Ni-UiO-66-NH_2@MWCNTs in 1 M KOH could be attributed to double layer capacitance (CPE_{dl} = 4289 µT) and high charge transfer resistance (R_{ct} = 176 Ω) on the electrode surface where no reaction is taking place. After addition of 1 M MeOH, the EIS revealed two smaller semicircles, where the first semicircle can be attributed to higher double layer capacitance (CPEdl = 1244 µT), as well as lower charge transfer resistance (R_{ct} = 14.94 Ω). The additional second semicircle can be correlated to the adsorption of methanol oxidation reaction intermediates onto the electrode surface with lower resistance (R_{ads} = 6.517 Ω and CPE_{ads} = 79.62 µT), thus confirming the methanol oxidation process on the catalyst surface [51]. Moreover, a fast mass transfer is evident by the presence of Warburg element, which indicates the fast oxidation process [29].

4 Conclusion

In summary, a simple one-pot synthesis method to prepare UiO-66-NH_2@MWCNTs followed by Ni^{2+} ion metalation through facile incipient wetness impregnation is presented, to generate a highly active electrocatalyst for alkaline methanol oxidation reaction. Electrochemical activation of the prepared composite resulted in NiOOH atop MWCNTs, which revealed exceptional electrocatalytic activity towards methanol oxidation in alkaline solution with appreciable stability. The Ni-UiO-66-NH_2@MWCNTs

Table 1 Electrochemical catalytic activity of reported MOF composites and MOF-derived catalysts towards methanol oxidation reaction

Catalyst	Electrolyte	MeOH conc. (M)	J (mA/cm^2)	Onset Potential (V vs Ag/AgCl)	Scan rate (mV/s^1)	Potential window (V)	Ref
$Ni_{0.6}Co_{0.4}$	1 M NaOH	0.5	116	0.42	50	0–1	[40]
Ni_{100} Bi_1 Nano-oxides	1 M NaOH	1	35	0.32	100	0–1	[41]
ZnO@C	1 M KOH	4	17	0.36	50	− 0.2 to 1	[42]
Ni_3Sn_2@CNFs	1 M KOH	1	68	0.32	50	00.8	[43]
PEDOT:PSS/MnO_2/rGO	0.5 M NaOH	0.5	56	0.32	50	− 0.35 to 0.35	[44]
Ni-NiO@C	1 M KOH	0.5	74	0.32[a]	50	0–0.7	[45]
MoS_2@CoNi-ZIF	1 M KOH	0.5	68	1.24[b]	50	0.8–1.6	[46]
Ni-Cu/TiN	1 M KOH	1	100	0.40	50	0–1	[47]
CoNi	0.1 M NaOH	0.1	3	0.42	20	0.1–0.7	[48]
Ni-UiO66-NH_2@MWCNTs	1 M KOH	1	**143**	**0.42**[c]	50	0–0.6	This Work

[a] vs SCE, [b] vs RHE, and [c] vs Hg/HgO

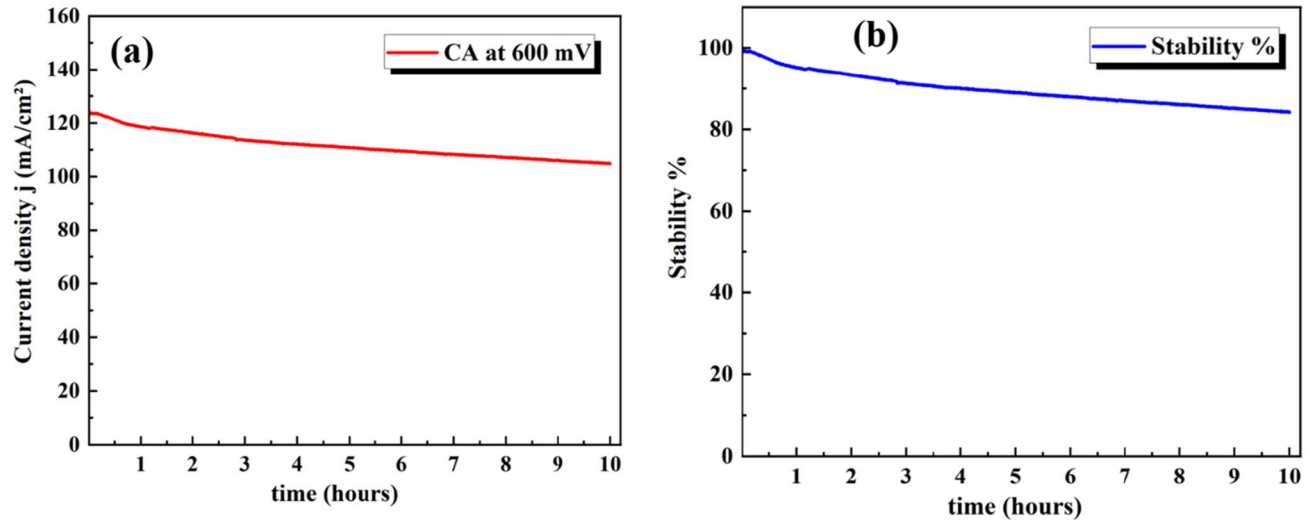

Fig. 9 (**a**) CA of Ni-UiO-66-NH_2@MWCNTs in 1 M KOH and 1 M MeOH at 0.6 V vs Hg/HgO after 10 h. (**b**) showing the stability after 10 h

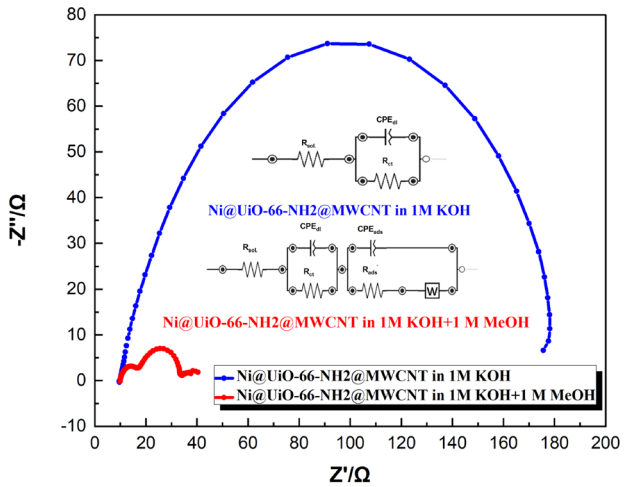

Fig. 10 Nyquist plots for Ni-UiO-66-NH2@MWCNTs at 0.6 V in 1 M KOH before and after addition of 1 M MeOH

catalyst retained 93.5% and 84.1% of the current density after 1 h and 10 h of continuous oxidation, respectively, and demonstrated superior catalytic activity and stability compared to other reported catalysts based on MOF composites/-derived catalysts. The reported approach opens the door for novel electrode materials for direct methanol fuel cell applications.

Acknowledgements This research was supported by the Academy of Scientific Research and Technology (ASRT) provided through a Science for Next Generation (SNG) cycle six (SGO-22) scholarship to Reham Shams-Eldin and (ASRT-APPLE) grant to Mohamed H. Alkordi.

Table 2 Fitting parameters of the different elements of the equivalent circuits used in modeling the EIS data for Ni-UiO-66-NH_2@MWCNTs in 1 M KOH before and after addition of 1 M MeOH

Element	Fitted values		Unit
	1 M KOH	1 M KOH + 1 M Methanol	
R_{sol}	9.877	9.890	Ω
CPE_{dl}	4289	1244	μT
n_1	0.857	0.913	ϕ
R_{ct}	176.5	14.94	Ω
CPE_{ads}	–	79.62	μT
n_2	–	0.844	ϕ
R_{ads}	–	6.517	Ω
W	–	0.001	kσ

Author contributions Reham Shams-Eldin conducted the synthesis, characterization, and electrochemical performance testing towards methanol oxidation and co-wrote the manuscript. Aya Ali conducted the EIS characterization and discussed the results. Amal Hani conducted literature review and co-writing the manuscript. Rana R. Haikal co-wrote and revised the manuscript. Hussein M. Fahmy, Rasha El Nashar and have revised the manuscript. Mohamed H. Alkordi conceived the idea, supervised the works, discussed the results, and co-writing the manuscript.

Funding Open access funding provided by The Science, Technology & Innovation Funding Authority (STDF) in cooperation with The Egyptian Knowledge Bank (EKB).

Data availability Original data is available from the corresponding author upon request.

Declarations

Conflict of interest There is no conflict to be declared.

Ethical approval Not Applicable.

References

1. George A, Olah AG, SuryaPrakash GK (2009) Beyond oil and gas: the methanol economy. Wiley, New York
2. Mousavi Z, Benvidi A, Jahanbani S, Mazloum-Ardakani M, Vafazadeh R, Zare HR (2016) Investigation of electrochemical oxidation of methanol at a carbon paste electrode modified with Ni(II)-BS complex and reduced graphene oxide nano sheets. Electroanalysis 28(12):2985–2992. https://doi.org/10.1002/elan.201501183
3. Cheung K-C, Wong W-L, Ma D-L, Lai T-S, Wong K-Y (2007) Transition metal complexes as electrocatalysts—development and applications in electro-oxidation reactions. Coord Chem Rev 251(17–20):2367–2385
4. Wang Y (2017) Methanol electrooxidation reaction in alkaline medium on glassy carbon electrode modified with ordered mesoporous Ni/Al2O3. Int J Electrochem Sci. https://doi.org/10.20964/2017.03.47
5. Choban ER, Spendelow JS, Gancs L, Wieckowski A, Kenis PJA (2005) Membraneless laminar flow-based micro fuel cells operating in alkaline, acidic, and acidic/alkaline media. Electrochim Acta 50(27):5390–5398. https://doi.org/10.1016/j.electacta.2005.03.019
6. Kwon Y, Lai SC, Rodriguez P, Koper MT (2011) Electrocatalytic oxidation of alcohols on gold in alkaline media: base or gold catalysis? J Am Chem Soc 133(18):6914–6917. https://doi.org/10.1021/ja200976j
7. Scott K, Xing L (2012) Direct methanol fuel cells. In: Fuel cell engineering. Advances in chemical engineering, pp 145–196. https://doi.org/10.1016/b978-0-12-386874-9.00005-1
8. Dong L, Gari RRS, Li Z, Craig MM, Hou S (2010) Graphene-supported platinum and platinum–ruthenium nanoparticles with high electrocatalytic activity for methanol and ethanol oxidation. Carbon 48(3):781–787. https://doi.org/10.1016/j.carbon.2009.10.027
9. Huang W, Wang H, Zhou J, Wang J, Duchesne PN, Muir D, Zhang P, Han N, Zhao F, Zeng M, Zhong J, Jin C, Li Y, Lee ST, Dai H (2015) Highly active and durable methanol oxidation electrocatalyst based on the synergy of platinum-nickel hydroxide-graphene. Nat Commun 6:10035. https://doi.org/10.1038/ncomms10035
10. Bai F, Sun Z, Wu H, Haddad RE, Xiao X, Fan H (2011) Templated photocatalytic synthesis of well-defined platinum hollow nanostructures with enhanced catalytic performance for methanol oxidation. Nano Lett 11(9):3759–3762. https://doi.org/10.1021/nl201799x
11. Lou Y, Maye MM, Han L, Luo J, Zhong C-J (2001) Gold–platinum alloy nanoparticle assembly as catalyst for methanol electrooxidation. Chem Commun 5:473–474. https://doi.org/10.1039/b008669j
12. Xiao S, Xiao F, Hu Y, Yuan S, Wang S, Qian L, Liu Y (2014) Hierarchical nanoporous gold-platinum with heterogeneous interfaces for methanol electrooxidation. Sci Rep 4:4370. https://doi.org/10.1038/srep04370
13. Zhao D, Xu BQ (2006) Enhancement of Pt utilization in electrocatalysts by using gold nanoparticles. Angew Chem Int Ed Engl 45(30):4955–4959. https://doi.org/10.1002/anie.200600155
14. Li J, Rong H, Tong X, Wang P, Chen T, Wang Z (2018) Platinum-silver alloyed octahedral nanocrystals as electrocatalyst for methanol oxidation reaction. J Colloid Interface Sci 513:251–257. https://doi.org/10.1016/j.jcis.2017.11.039
15. Xia Z, Xu X, Zhang X, Li H, Wang S, Sun G (2020) Anodic engineering towards high-performance direct methanol fuel cells with non-precious-metal cathode catalysts. J Mater Chem A 8(3):1113–1119
16. Gopalakrishnan A, Durai L, Ma J, Kong CY, Badhulika S (2021) Vertically aligned few-layer crumpled MoS2 hybrid nanostructure on porous Ni foam toward promising binder-free methanol electro-oxidation application. Energy Fuels 35(12):10169–10180
17. Pettinari C, Marchetti F, Mosca N, Tosi G, Drozdov A (2017) Application of metal– organic frameworks. Polym Int 66(6):731–744
18. Markus J. Kalmutzki1 NH, Omar M. Yaghi (2018) Secondary building units as the turning point in the development of the reticular chemistry of MOFs. Sci Adv 4
19. M. Fleischmann KK, and D. Pletcher (1972) The Kinetics and Mechanism of the Oxidation of Amines and Alcohols at Oxide-covered Nickel, Silver, Copper, and Cobalt Electrodes. J Chem Soc, Perkin Trans 2
20. Wang W, Li R, Zhang R, Ma J, Wang B (2015) Electrocatalytic oxidation of methanol on glassy carbon electrode modified with nickel–manganese salen complexes encapsulated in mesoporous zeolite A. J Electroanal Chem 742:110–121. https://doi.org/10.1016/j.jelechem.2015.01.036
21. Morozan A, Jaouen F (2012) Metal organic frameworks for electrochemical applications. Energy Environ Sci. https://doi.org/10.1039/c2ee22989g
22. Jaouen F, Morozan A (2014) Metal-organic frameworks: electrochemical properties. In: Encyclopedia of inorganic and bioinorganic chemistry, pp 1–24. https://doi.org/10.1002/9781119951438.eibc2226
23. Li J-H, Wang Y-S, Chen Y-C, Kung C-W (2019) Metal–organic frameworks toward electrocatalytic applications. Appl Sci. https://doi.org/10.3390/app9122427
24. Wang N, Liang S, Zhang L, Cao P, Xu L, Lin M (2020) Ionic liquid supported nickel-based metal-organic framework for electrochemical sensing of hydrogen peroxide and electrocatalytic oxidation of methanol. Colloids Surf A. https://doi.org/10.1016/j.colsurfa.2020.125199
25. Hoseini SJ, Bahrami M, Nabavizadeh SM (2019) ZIF-8 nanoparticles thin film at an oil–water interface as an electrocatalyst for the methanol oxidation reaction without the application of noble metals. New J Chem 43(39):15811–15822. https://doi.org/10.1039/c9nj02855b
26. Yaqoob L, Noor T, Iqbal N, Nasir H, Zaman N (2019) Development of Nickel-BTC-MOF-Derived Nanocomposites with rGO Towards Electrocatalytic Oxidation of Methanol and Its Product Analysis. Catalysts. https://doi.org/10.3390/catal9100856

27. Rezaee S, Shahrokhian S (2019) Facile synthesis of petal-like NiCo/NiO-CoO/nanoporous carbon composite based on mixed-metallic MOFs and their application for electrocatalytic oxidation of methanol. Appl Catal B 244:802–813
28. Qian L, Luo S, Wu L, Hu X, Chen W, Wang X (2020) In situ growth of metal organic frameworks derived hierarchical hollow porous Co3O4/NiCo2O4 nanocomposites on nickel foam as self-supported flexible electrode for methanol electrocatalytic oxidation. Appl Surf Sci. https://doi.org/10.1016/j.apsusc.2019.144306
29. Sheikhi S, Jalali F (2021) Remarkable electrocatalytic activity of Ni-nanoparticles on MOF-derived ZrO2-porous carbon/reduced graphene oxide towards methanol oxidation. Int J Hydrogen Energy 46(18):10723–10738. https://doi.org/10.1016/j.ijhydene.2020.12.168
30. Meenu PC, Datta SP, Singh SA, Dinda S, Chakraborty C, Roy S (2021) A compendium on metal organic framework materials and their derivatives as electrocatalyst for methanol oxidation reaction. Mol Catal. https://doi.org/10.1016/j.mcat.2021.111710
31. Mehek R, Iqbal N, Noor T, Nasir H, Mehmood Y, Ahmed S (2017) Novel Co-MOF/graphene oxide electrocatalyst for methanol oxidation. Electrochim Acta 255:195–204
32. Yaqoob L, Noor T, Iqbal N, Nasir H, Zaman N, Rasheed L, Yousuf M (2020) Development of an efficient non-noble metal based anode electrocatalyst to promote methanol oxidation activity in DMFC. ChemistrySelect 5(20):6023–6034. https://doi.org/10.1002/slct.202000705
33. Hassan MH, Haikal RR, Alkordi MH (2022) Synergistic compounding of carbon nanotubes and metal–organic frameworks for oxygen-evolving electrocatalysis. Materials Advances 3(19):7212–7218
34. Ibrahim AH, Haikal RR, Eldin RS, El-Mehalmey WA, Alkordi MH (2021) The role of free-radical pathway in catalytic dye degradation by hydrogen peroxide on the Zr-based UiO-66-NH2 MOF. ChemistrySelect 6(42):11675–11681
35. Baker AM, Wang L, Advani SG, Prasad AK (2012) Nafion membranes reinforced with magnetically controlled Fe 3 O 4–MWCNTs for PEMFCs. J Mater Chem 22(28):14008–14012
36. Cavka JH, Jakobsen S, Olsbye U, Guillou N, Lamberti C, Bordiga S, Lillerud KP (2008) A new zirconium inorganic building brick forming metal organic frameworks with exceptional stability. J Am Chem Soc 130(42):13850–13851
37. Sonia Theres G, Velayutham G, Santhana Krishnan P, Shanthi K (2019) Synergistic impact of Ni–Cu hybrid oxides deposited on ordered mesoporous carbon scaffolds as non-noble catalyst for methanol oxidation. J Mater Sci 54(2):1502–1519
38. Sheikhi S, Jalali F (2021) Zr-MOF@ Polyaniline as an efficient platform for nickel deposition: Application to methanol electrooxidation. Fuel 296:120677
39. Tomboc GM, Abebe MW, Baye AF, Kim H (2019) Utilization of the superior properties of highly mesoporous PVP modified NiCo2O4 with accessible 3D nanostructure and flower-like morphology towards electrochemical methanol oxidation reaction. J Energy Chem 29:136–146
40. Que R, Li M, Yao H, Wang X, Liao F, Shao M (2020) Unusual effect of trace water on the structure and activity of Nix Co1-x electrocatalysts for the methanol oxidation reaction. Chemsuschem 13(5):964–973. https://doi.org/10.1002/cssc.201903108
41. Gao P, Gu Y, Li P, Yu Z, Hu Y, Zhang C, Xu Z, An Y (2020) Promoting effect of Bi in Ni–Bi oxide electrocatalysts for methanol oxidation reaction. J Mater Sci Mater Electron 31(16):13219–13228. https://doi.org/10.1007/s10854-020-03873-y
42. Ghouri ZK, Al-Meer S, Barakat NAM, Kim HY (2017) ZnO@C (core@shell) microspheres derived from spent coffee grounds as applicable non-precious electrode material for DMFCs. Sci Rep 7(1):1738. https://doi.org/10.1038/s41598-017-01463-3
43. Barakat NAM, Al-Mubaddel FS, Rezual Karim M, Alrashed M, Yong Kim H (2018) Influence of Sn content on the electrocatalytic activity of NiSn alloy nanoparticles-incorporated carbon nanofibers toward methanol oxidation. Int J Hydrogen Energy 43(46):21333–21344. https://doi.org/10.1016/j.ijhydene.2018.09.196
44. Baruah B, Kumar A (2018) PEDOT:PSS/MnO2/rGO ternary nanocomposite based anode catalyst for enhanced electrocatalytic activity of methanol oxidation for direct methanol fuel cell. Synth Met 245:74–86. https://doi.org/10.1016/j.synthmet.2018.08.009
45. Yu J, Ni Y, Zhai M (2018) Simple solution-combustion synthesis of Ni-NiO@C nanocomposites with highly electrocatalytic activity for methanol oxidation. J Phys Chem Solids 112:119–126. https://doi.org/10.1016/j.jpcs.2017.09.022
46. Liu Y, Hu B, Wu S, Wang M, Zhang Z, Cui B, He L, Du M (2019) Hierarchical nanocomposite electrocatalyst of bimetallic zeolitic imidazolate framework and MoS2 sheets for non-Pt methanol oxidation and water splitting. Appl Catal B. https://doi.org/10.1016/j.apcatb.2019.117970
47. Mao Y-H, Chen C-Y, Fu J-X, Lai T-Y, Lu F-H, Tsai Y-C (2018) Electrodeposition of nickel-copper on titanium nitride for methanol electrooxidation. Surf Coat Technol 350:949–953. https://doi.org/10.1016/j.surfcoat.2018.03.048
48. Tarrús X, Montiel M, Vallés E, Gómez E (2014) Electrocatalytic oxidation of methanol on CoNi electrodeposited materials. Int J Hydrogen Energy 39(12):6705–6713. https://doi.org/10.1016/j.ijhydene.2014.02.057
49. Müller JT, Urban PM, Hölderich WF (1999) Impedance studies on direct methanol fuel cell anodes. J Power Sources 84(2):157–160. https://doi.org/10.1016/S0378-7753(99)00331-6
50. Seo SH, Lee CS (2008) Impedance characteristics of the direct methanol fuel cell under various operating conditions. Energy Fuels 22(2):1204–1211
51. Danaee I, Jafarian M, Forouzandeh F, Gobal F, Mahjani MG (2009) Electrochemical impedance studies of methanol oxidation on GC/Ni and GC/NiCu electrode. Int J Hydrogen Energy 34(2):859–869. https://doi.org/10.1016/j.ijhydene.2008.10.067